# Theoretical approaches to charged surfaces



2004 J. Phys.: Condens. Matter 16 S2353

(http://iopscience.iop.org/0953-8984/16/26/009)

INSTITUTE OF PHYSICS PUBLISHING JOURNAL OF PHYSICS: CONDENSED MATTER

J. Phys.: Condens. Matter **16** (2004) S2353–S2368 PII: S0953-8984(04)78572-0

# Theoretical approaches to charged surfaces

**R R Netz**

Sektion Physik, LMU Munich, Theresienstraße 37, 80333 Munich, Germany
and
Centre for Nanoscience, LMU Munich, Geschwister-Scholl Platz 1, 80799 Munich, Germany

E-mail: netz@theorie.physik.uni-muenchen.de

Received 27 March 2004
Published 18 June 2004
Online at stacks.iop.org/JPhysCM/16/S2353
doi:10.1088/0953-8984/16/26/009

**Abstract**

We summarize some of our recent theoretical and numerical work on the behaviour and structure of charged surfaces. Due to the coupling of effects on vastly different length scales, a complete treatment of charged surfaces is out of reach with present computer power. On the other hand, some progress can and has been made by concentrating on one specific aspect at a time with a suitably chosen numerical method. We discuss four such calculations, each using a different computational scheme, that yield various levels of description of charged surfaces. (i) Coarse grained Monte Carlo simulations of idealized surfaces incorporate large-length-scale fluctuation and correlation effects in the counterion cloud at a charged surface. (ii) Brownian dynamics simulations of more realistic, structured surfaces give modified counterion distributions and also allow one to estimate dynamic and non-equilibrium quantities such as the mobility of counterions at charged surfaces. (iii) All-atomistic molecular dynamics simulations of water at surfaces correctly reproduce water structuring effects at surfaces such as hydration and hydrophobic dewetting. (iv) On the nanoscopic level, quantum mechanical *ab initio* calculations give the effective interactions between oppositely charged groups in vacuum and in solution. The real theoretical challenge is to correctly piece together results obtained on all these different length scales.

(Some figures in this article are in colour only in the electronic version)

## 1. Introduction

Although a lot of theoretical and experimental work has been aimed at elucidating the behaviour of charged surfaces, many questions remain unanswered and we are still far from a complete understanding [1–5]. The reasons for this are many:

(i) Charged systems are typically aqueous systems, and the behaviour of water at surfaces is complicated in itself and not fully understood.

  

(ii) Oppositely charged groups or ions are pushed together by Coulombic attraction; as a result of the small separations, quantum effects come into play and make the interaction between oppositely charged ions highly specific.
(iii) Collective behaviour of charged ions at an oppositely charged surface arises since the degrees of freedom of all ions are coupled via the long-ranged Coulomb interaction and leads to large-wavelength correlations.

It is the mixture of all these effects, each operative at a different length scale, that makes the problem of charged surfaces intractable on the *ab initio* level with present computer power. Nevertheless, progress has been made in the last few years by concentrating on certain aspects at a time, leaving aside the other complications. As examples of such approaches, we briefly review four different simulations which are concerned with very different length scales and aspects of charged surfaces:

(i) Recently, coarse grained Monte Carlo simulations were performed for charged ions at oppositely charged, smooth surfaces within the so-called primitive model (which leaves aside effects such as water structure and specific ion interactions). Here the large-length-scale properties can be analysed and, more specifically, deviations from the classical Poisson–Boltzmann equation can be quantified.
(ii) More detailed Brownian dynamics simulations take into account the substrate surface structure and also allow one to estimate mobilities of ions.
(iii) Molecular dynamics simulations of water at hydrophobic substrates reveal that such substrates induce formation of a thin layer within which the water is depleted from the wall. Many charged surfaces are of hydrophobic nature, and it is suggested that these water structuring effects at surfaces are important since they will influence the degree of surface-group dissociation and the interactions with counterions.
(iv) Finally, at the smallest length scale, the interaction between oppositely charged ions has been studied using *ab initio* quantum chemistry calculations.

As mentioned before, each of these four simulation techniques is capable of dealing with one aspect of charged surfaces, but necessarily leaves aside other aspects. Quantum chemistry techniques can be used for calculations for molecules or small clusters of molecules on a basically *ab initio* level, but are not suited for looking at counterion density distributions or other large-length-scale effects. Molecular dynamics simulations yield structural and dynamic properties of larger systems, assuming a fixed set of heuristically determined force fields, but the maximal system size and the maximal simulation time are smaller than one would need for many applications. Finally, Monte Carlo methods and Brownian dynamics simulations allow one to go to large system sizes and also large timescales; the price one pays for this is simplistic models which neglect most of microscopic details, and a neglect of the short-timescale behaviour. The future challenges will be allowing for cross-fertilization between these various approaches and designing reliable hybrid simulation techniques which combine the strengths of more than one of them.

## 2. Charged smooth surfaces

A great deal of work has been devoted in the past twenty years to understanding the interaction between two charged surfaces. Specifically, it has been known for some time that two similarly and strongly charged plates can attract each other in the presence of multivalent counterions or even with monovalent counterions when the surface charge density is extremely high [6]. This contradicts the standard mean-field theory for charged systems, called Poisson–Boltzmann theory, which predicts the pressure between similarly charged surfaces to be repulsive.

Experimentally, the interaction between charged planar objects can be very elegantly studied using a stack of charged, self-assembled membranes. Such membranes spontaneously form in aqueous solution of charged amphiphilic molecules (lipids or surfactants) and consist of bilayers which are separated by water slabs [7–9]. Since the membranes are highly charged (they typically contain one surface charge per 0.6 nm$^2$ and thus are among the most highly charged surfaces known), one would expect strong repulsion between them, or, which is equivalent, a strongly positive and monotonically decaying osmotic pressure in such a stack. In contrast, experiments using the cationic surfactant DDAB show that a mysterious attraction exists between the charged lamellae [8, 9]. We should add that a similar attraction is also seen with less strongly charged bilayer systems when the monovalent counterions are replaced by divalent counterions [10, 11].

The following points are important for the present discussion. For each surface charge an oppositely charged counterion is released into the aqueous solution. These counterions form clouds that are loosely bound to the surface charges. The interactions between charged bodies and their electric properties themselves (such as their electrophoretic mobility in an electric driving field) are predominantly determined by the properties of these counterion clouds, and an understanding of the behaviour of charged bodies requires an understanding of the counterion clouds to be achieved first. As it turns out, the experimentally observed attraction between similarly charged surfaces requires a deeper understanding of counterion layers at highly charged surfaces. In the following, we concentrate on a single, planar charged surface with counterions only, i.e. no additional salt ions (the case of two charged walls has been discussed at length in [12–14]).

The strategy is to formulate the simplest model which captures the electrostatic correlation effects which are believed to be at the heart of the like-charge attraction. The Hamiltonian for a system of $N$ pointlike counterions of valence $q$, located at positions $\mathbf{r}_i$, close to a single oppositely charged planar and homogeneous wall of charge density $\sigma_s$, is (in units of $k_BT$) given by

$$\mathcal{H} = \sum_{j=1}^{N-1} \sum_{k=j+1}^{N} \frac{q^2 \ell_B}{|\mathbf{r}_j - \mathbf{r}_k|} + 2\pi q \ell_B \sigma_s \sum_{j=1}^{N} z_j, \tag{1}$$

where $\ell_B \equiv e^2/4\pi\varepsilon\varepsilon_0 k_B T$ is the Bjerrum length ($e$ is the elementary charge, $\varepsilon$ is the relative dielectric constant). In water, one typically has $\ell_B \approx 0.7$ nm. The first term contains the Coulombic repulsion between all ions; the second term accounts for the electrostatic attraction to the wall (which is assumed to be of infinite lateral extent and located in the $z = 0$ plane). The relevant length scale in the system is the Gouy–Chapman length, $\mu$, i.e., the distance from the charged wall at which the potential energy of one isolated counterion equals the thermal energy $k_BT$, which is a measure of the typical height of the counterion layer. From equation (1) it can be read off as

$$\mu = \frac{1}{2\pi q \ell_B \sigma_s}. \tag{2}$$

If one expresses all lengths in units of the Gouy–Chapman length according to

$$\tilde{r} = r/\mu, \tag{3}$$

the Hamiltonian equation (1) can be rewritten as

$$\mathcal{H} = \sum_{j=1}^{N-1} \sum_{k=j+1}^{N} \frac{\Xi}{|\tilde{\mathbf{r}}_j - \tilde{\mathbf{r}}_k|} + \sum_{j=1}^{N} \tilde{z}_j. \tag{4}$$

Now the Hamiltonian only depends on a single parameter, the coupling parameter

$$\Xi = 2\pi q^3 \ell_B^2 \sigma_s \sim \frac{q^3 \sigma_s}{T^2}, \tag{5}$$

which includes the effects of varying temperature $T$ (via the Bjerrum length $\ell_B$), surface charge density $\sigma_s$, and counterion valence $q$. The counterion valence enters the coupling parameter as a cube, showing that this is an experimental parameter which decisively controls the resultant behaviour of the double layer (compare the experiments with charged lamellar systems where the counterion valency has been increased [10, 11]). Small values of $\Xi$ define the weak-coupling regime (where, as has been demonstrated, the mean-field Poisson–Boltzmann (PB) theory becomes valid); large values define the strong-coupling (SC) regime, which constitutes a sound physical limit with behaviour very different from that at the PB limit [15, 16]. This can already be appreciated from a simple geometric scaling argument, which is presented in the following.

The mean lateral area per counterion is determined by the surface charge density and defines a length scale (which we associate with the lateral distance between ions), $a_\perp$, via the relation

$$\pi a_\perp^2 = q/\sigma_s. \tag{6}$$

In rescaled units, this lateral distance reads

$$\tilde{a}_\perp = a_\perp/\mu = \sqrt{2\Xi}. \tag{7}$$

Since, as we will see shortly, the height of the bound counterion cloud is unity in reduced units, it follows from equation (7) that for coupling parameters larger than unity, $\Xi > 1$, the lateral distance between ions is larger than their separation from the wall and thus the layer is essentially flat and two dimensional [17, 18]. For $\Xi < 1$, on the other hand, the lateral ion separation $a_\perp$ is smaller than the layer height $\mu$, which means that within the counterion layer the ion–ion correlations should be rather 3D fluidlike. This is demonstrated in figure 1, where we show snapshots of counterion distributions obtained in Monte Carlo simulations for two different values of the coupling parameter, $\Xi = 1$ and 100. For small $\Xi$, the ion distribution is indeed rather diffuse and disordered and mean-field theory should work, since each ion moves in a weakly varying potential due to the diffuse cloud of neighbouring ions. For large $\Xi$, on the other hand, ion–ion distances are large compared to the distance from the wall; the ions form a flat layer on the charged wall. A two-dimensional one-component plasma is known to crystallize for a value of the coupling parameter of $\Xi \approx 31\,000$, suggesting that both snapshots shown in figure 1 are for coupling constants far below the crystallization threshold. However, mean-field theory is expected to break down, at least for the system with $\Xi = 100$, because each ion moves, though confined by its immediate neighbours in the lateral directions, almost independently from the other ions along the vertical direction (which constitutes the soft mode). We stress that this continuous crossover from a three-dimensional disordered counterion distribution for small $\Xi$ to a two-dimensional correlated counterion distribution for large $\Xi$ is a pure consequence of the scaling analysis; it requires the rescaled counterion layer height, as the only input, to be of order unity, which is true irrespective of the precise value of $\Xi$, as we will demonstrate next.

Using Monte Carlo simulation techniques, we have obtained counterion density profiles by averaging over subsequent counterion configurations for different values of $\Xi$. Since the surface charge density is homogeneous, the counterion density profile $\rho(z)$ only depends on the distance from the wall, $z$. The counterions exactly neutralize the surface charges; the integral over the counterion density profile is therefore given by (in unrescaled units)

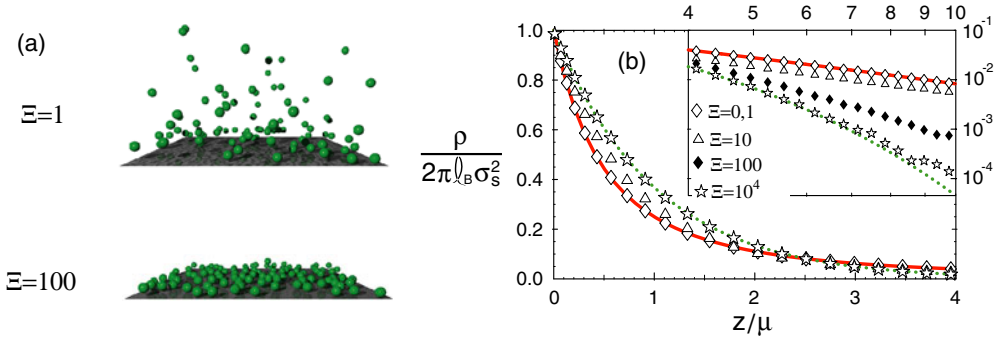


**Figure 1.** (a) Snapshots of counterion distributions at a charged surface for two different values of the coupling parameter, showing a rather diffuse distribution for small $\Xi$ and a flat quasi-two-dimensional layer for large $\Xi$. (b) Numerically determined counterion density profiles (data points) as a function of the distance from the surface for different values of the coupling parameter $\Xi$ in comparison with the asymptotic predictions in the mean-field (solid curve) and strong-coupling (broken curve) limits (adapted from [15]).

$\int_0^\infty \mathrm{d}z\, \rho(z) = \sigma_\mathrm{s}/q$. Using the rescaled distance coordinate $\tilde{z} = z/\mu$, the integral gives $\int_0^\infty \mathrm{d}\tilde{z}\, \rho(\tilde{z}) = 2\pi\ell_\mathrm{B}\sigma_\mathrm{s}^2$, which suggests defining the rescaled density profile as

$$\tilde{\rho}(\tilde{z}) = \frac{\rho(\tilde{z})}{2\pi\ell_\mathrm{B}\sigma_\mathrm{s}^2} \tag{8}$$

which, via the condition of electroneutrality, is normalized to unity:

$$\int_0^\infty \mathrm{d}\tilde{z}\, \tilde{\rho}(\tilde{z}) = 1. \tag{9}$$

In figure 1 we show rescaled counterion density profiles obtained using Monte Carlo simulations for various values of the coupling parameter $\Xi = 0.1$, 10, 100, and $10^4$. One notes that all profiles saturate at a rescaled density of unity at the charged wall. This is in accord with the contact-value theorem, which states that the counterion density at the wall is—for the case of a single homogeneously charged wall—exactly given by $\rho(0) = 2\pi\ell_\mathrm{B}\sigma_\mathrm{s}^2$ or, in rescaled units,

$$\tilde{\rho}(0) = 1 \tag{10}$$

(incidentally in agreement with the Poisson–Boltzmann prediction). Given the two constraints on the rescaled density profile, namely being normalized to unity and reaching a contact density of unity at the wall, equations (9) and (10), it is clear that the profiles in the units chosen by us have to be quite similar to each other even for vastly different coupling parameters, as is indeed observed in figure 1. Also, it is a rather trivial consequence of both constraints that the typical decay length of the profiles is always given by unity in rescaled units (though, strictly speaking, the first moment $\langle\tilde{z}\rangle$ of the density distribution diverges logarithmically within PB theory). Still, the asymptotic predictions for vanishing coupling constant ($\Xi \to 0$, PB theory, solid curve in figure 1) and diverging coupling constant ($\Xi \to \infty$, SC theory, broken curve) are as different as they can be from a functional point of view, while still obeying the constraints mentioned above, as we will now recapitulate.

At low coupling, the counterion density distribution is well described by the Poisson–Boltzmann (PB) theory, which predicts an algebraic decay: profile [19–21]

$$\tilde{\rho}_\mathrm{PB}(\tilde{z}) = \frac{1}{(1+\tilde{z})^2}, \tag{11}$$

shown in figure 1(b) as a solid curve, while in the opposite limit of high coupling, the strong-coupling (SC) theory, predicting an exponential decay profile [15, 13]

$$\tilde{\rho}_{\mathrm{SC}}(\tilde{z}) = \exp(-\tilde{z}), \tag{12}$$

shown in figure 1(b) as a broken curve, becomes asymptotically exact. An exponential density profile (although with a different pre-factor) has also been obtained by Shklovskii [18] using a heuristic model for a highly charged surface, where counterions bound to the wall are in chemical equilibrium with free counterions. The intuitive explanation for the exponential density profile equation (12) uses the fact that for large values of the coupling constant a counterion mostly interacts with the charged wall and therefore experiences a linear wall potential, the second term in equation (4), with only small corrections due to other ions. The single-ion distribution function follows by exponentiating the wall potential, similar to the derivation of the barometric height formula for the atmospheric density, and in agreement with the result in equation (12). It is important to note, though, that equation (12) has been obtained as the leading term in a systematic field-theoretic derivation which also gives correction terms [13] which in turn have been favourably compared with simulation results [14]. As can be seen from figure 1, the PB density profile equation (11) is only realized for $\Xi < 1$, while the strong-coupling profile equation (12) is indeed the asymptotic solution and agrees with simulation results for $\Xi > 10^4$ over the distance range considered in the simulations. In fact, there is a crossover between the two asymptotic theories which is distance dependent, which is discussed in detail in [13, 14]. In summary, the strong-coupling theory is a theory that becomes asymptotically exact in the opposite limit when the mean-field or Poisson–Boltzmann theory is valid. The two theories therefore describe the two extreme situations.

Experimentally, a coupling parameter $\Xi = 100$, which is already quite close to the strong-coupling limit, is reached with divalent ions for a surface charge density $\sigma_{\mathrm{s}} \approx 3.9\ \mathrm{nm}^{-2}$, which is feasible with compressed charged monolayers, and with trivalent counterions for $\sigma_{\mathrm{s}} \approx 1.2\ \mathrm{nm}^{-2}$, which is a typical value. The strong-coupling limit is therefore experimentally accessible and not just interesting from a fundamental point of view.

We finish this section by noting that for the case of two charged plates, the PB theory predicts that the pressure is always positive (only repulsion), while the SC theory gives attraction, in agreement with MC simulations [12, 14] and experiments [8–11].

## 3. Charged structured surfaces

In the previous section we looked at the somewhat artificial model where the charged surface is smooth and homogeneously charged, and where the counterions are pointlike and thus only interact via Coulomb interactions. In reality, even an atomically flat surface exhibits some degree of corrugation, and counterions have a finite extent and thus experience some type of excluded-volume interaction.

In this section we consider a two-dimensional layer of $N$ charged spheres of valency $q$ and diameter $a$ (at $z = 0$), together with $N$ oppositely charged counterions of the same valency and diameter, which are confined to the upper half-space ($z > 0$) in a cubic simulation box of length $L$ (see figure 2(a)). The number density of surface ions is $\rho_{\mathrm{s}} = N/L^2$. The other important parameter is $\zeta = q^2 \ell_{\mathrm{B}}/a$ which measures the ratio of the Coulomb interaction and the thermal energy at the minimal distance $a$. Collapse of counterions and surface ions is prevented by a truncated Lennard-Jones term acting between all particles. The model we consider includes the combined effects of discrete surface charges, surface corrugations, and the counterion excluded volume [22], which are all neglected in the classical mean-field approaches. As the simulation technique we employ a Brownian dynamics simulation where the velocity of all particles

follows from the position Langevin equation. The proper canonical distribution functions are obtained by adding a suitably chosen Gaussian noise force acting on all particles. Averages are obtained by averaging particle trajectories over time. In figure 2(b) we show a snapshot of the counterion configuration obtained during a simulation. In figures 2(c) and (d) we show laterally averaged counterion density profiles for fixed Coulomb strength $\zeta = 2.5$ and various surface ion densities. This Coulomb strength corresponds to a distance of closest approach between ions of 3 Å which is a quite realistic value for normal ions. We also show the mean-field (MF) prediction for the laterally homogeneous case, equation (11), which reads in normalized form $\rho(z)/\rho_s = \mu^{-1}/(1 + z/\mu)^2$. As before, the Gouy–Chapman length $\mu = a/(2\pi\zeta a^2\rho_s)$ is a measure of the decay length of the profiles. For small surface ion densities, figure 2(c), the measured profiles agree quite well with the MF predictions, as expected, since the Gouy–Chapman length is larger than the lateral surface ion separation and the charge modulation and hard-core repulsion matter little. However, even for the smallest density considered (open squares) there are some deviations in the distance range $z/a < 1$ which we attribute to the hard-core repulsion between surface ions and counterions [16]. For the larger surface densities in figure 2(d) the deviations become more pronounced (simply shifting the MF profiles does not lead to satisfactory agreement). For $\rho_s a^2 = 0.5$ (open diamonds) some counterions still reach the surface at $z = 0$, but the profile is considerably shifted to larger values of $z$ due to the impenetrability of surface ions and counterions. Finally, for $\rho_s a^2 = 2$ (filled triangles) the surface ions form an impenetrable but highly corrugated layer, and the counterion profile is shifted by almost an ion diameter outwards (and a second layer of counterions forms). These results remind us that in experimental systems a number of effects are present which make comparison with theories based on laterally homogeneous charge distributions difficult. As an aside, we note that the coupling constant $\Xi = 2\pi\rho_s a^2\zeta^2$ (which measures deviations from MF theory due to fluctuations and correlations; see the previous section) is for the data in figure 2(d) in a range where deviations from MF theory are becoming noticeable for the smeared-out case [15]; for $\rho_s a^2 = 2$ one finds $\Xi \approx 75$ which means that Poisson–Boltzmann theory is invalid for almost all relevant surface distances. But it is important to note that the deviations from Poisson–Boltzmann theory that we talked about in the previous section, as illustrated in figure 1(b) for smooth substrates, are totally overwhelmed by the more drastic effects illustrated in figure 2. The big advantage of the Brownian dynamics technique is that dynamic quantities can be calculated. In the present example, the counterion mobility with respect to a tangential field is greatly reduced by the presence of surface corrugation [22], which can be understood since counterions are dynamically trapped within the surface charge layer. This might explain a whole collection of experimental results on the electrophoretic mobility of charged colloids.

## 4. Water at hydrophobic substrates

In the simplified models introduced in the two previous sections the presence of water was accounted for only by the fact that the relative dielectric constant is $\varepsilon = 78$. As is routinely done in most theoretical considerations, no other water effects are included, which is a highly questionable concept, as will be discussed now.

For very large non-polar objects or in the limiting case of a planar hydrophobic substrate in contact with water, it has been known for a long time that the water density is reduced at the hydrophobic surface [23, 24]. It seems fair to say that without a proper characterization of the behaviour of water at hydrophobic surfaces, no true understanding of the properties of such surfaces and their interactions will be possible. Quite possibly, many of the features interpreted as being inherent to surfaces themselves might in fact reflect properties of the

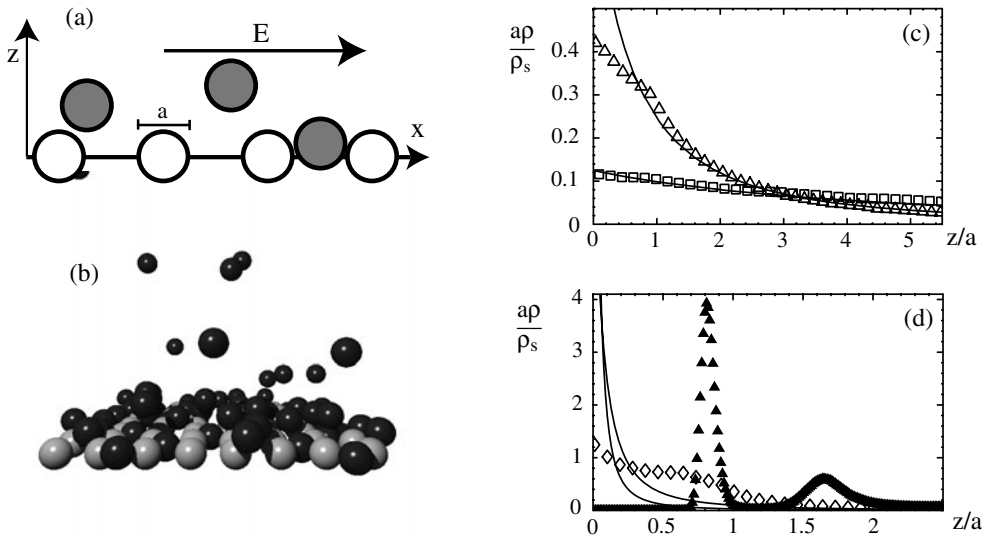


**Figure 2.** (a) In the simulations a two-dimensional layer of fixed surface ions is in contact with oppositely charged counterions of the same diameter $a$ and valency $q$. (b) A snapshot of an ion configuration for a surface density $\rho_s a^2 = 0.5$ and Coulomb coupling $\zeta = 2.5$. (c) Laterally averaged counterion density profiles for Coulomb coupling $\zeta = 2.5$ as a function of the rescaled distance from the surface (surface ions are fixed on a square lattice). Shown here are results for surface ion densities (c) $\rho_s a^2 = 0.0079$ (open squares), $\rho_s a^2 = 0.05$ (open triangles), (d) $\rho_s a^2 = 0.5$ (open diamonds), $\rho_s a^2 = 2$ (filled triangles), together with the mean-field predictions for the laterally homogeneous case (solid curves).

interfacial water layer instead (e.g. protein adsorption resistivity [25], zeta potentials [26], surface potentials [27], polymer adsorption energies [28], to mention just a few). We will now consider the water density profile close to a planar surface using molecular dynamics (MD) simulations. In MD simulations, one basically integrates Newton's equation of motion for an assembly of molecules or atoms, using heuristically chosen force parametrizations. The constant pressure ensemble is realized by adjusting the system volume. For simplicity, we only consider neutral walls, and in order to bring out the consequences of the presence of a wall clearly, we deal with the special case of a very hydrophobic wall.

The work described here was motivated by recent scattering experiments where the water density depletion at planar non-polar substrates was determined. As the main result of those experiments, it was shown that the effective depletion thickness (defined as the thickness of a steplike depletion layer consisting of vacuum with the same integrated depleted amount as the rounded and smeared-out depletion profiles found in experiments) is roughly 2.5 Å on hydrophobic polystyrene substrates [29] and 5 Å on hydrophobic self-assembled monolayers [30], using neutron reflectivity methods, and about 1 Å on paraffin substrates, using x-ray reflectivity measurements [31]. Ellipsometry measurements point to a depletion thickness of about 2–3 Å [32]. The reason for the discrepancies among different experiments is not well understood, but since the strength of water hydration depends on the radius of curvature of the solutes, it is clear that surface roughness is one important factor (among many others, e.g. small traces of attractive interactions between walls and water molecules) and will, if present, reduce the depletion.

In the simulations, we built up the hydrophobic substrate from self-assembled alkane chains which seems to be an acceptable representation of the substrate structure used in recent

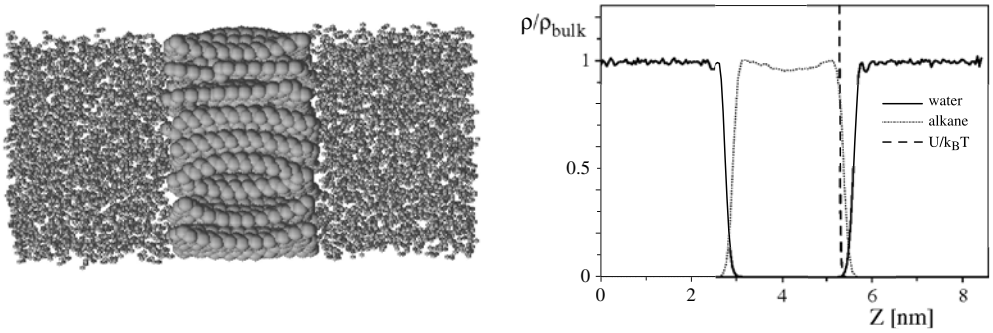


**Figure 3.** To the left: a snapshot of the MD simulation of a planar hydrophobic slab (made up of 64 alkane molecules) in contact with a water slab, consisting of 2781 SPC/E water molecules. To the right: a normalized density profile of the hydrophobic alkane slab (dotted curve, in the middle) and the water layers (solid curve, to the left and to the right) at constant pressure of 1 bar and temperature $T = 300$ K. The broken line denotes $U(z)/k_{\mathrm{B}}T$, the laterally averaged Lennard-Jones potential felt by the water molecules. The system was thermalized for 100 ps and averaged for 2 ns.

experiments [29–31]. In figure 3 to the left a snapshot of the MD simulation is shown, which serves to illustrate the geometry of the system [33]. The alkane molecules form a compact slab in the middle of the simulation box. They are only allowed to fluctuate in the $z$-direction and thus allow fast pressure equilibration. The water slab has a thickness of about 4 nm, which should be large enough that bulk water properties are reproduced. We therefore interpret our results as being caused by the single hydrophobic substrate–water interface and neglect interactions between the two interfaces through the finite water slab.

In figure 3 to the right we show the normalized densities of the alkane slab (dotted curve) and the water layer (solid curve) at atmospheric pressure and at a temperature $T = 300$ K. It is clearly seen that between the alkane slab and the water layer a region of reduced density appears. The density profiles are calculated using pointlike atomic form factors and denote the nuclear density; they therefore correspond to what would be seen in a neutron scattering experiment. The broken line denotes the laterally averaged interaction potential due to the alkane slab; in other words, this is the potential energy felt by the water molecules. At room temperature and normal pressure, we obtain for the depletion thickness of a planar hydrophobic substrate the value $d_2 = 2.565$ Å, which is of the order of the length obtained in recent neutron scattering experiments [29, 30] and twice the length obtained with x-rays at hydrophobic substrates [31].

What do these results imply for charged surfaces? Many of the charged surfaces used in experiments are in fact, if one forgets about the charged groups for a moment, of hydrophobic nature. A layer of reduced water density at such surfaces means that the effective dielectric constant is reduced, which in turn suggests that the association–dissociation equilibrium of surface charges will be perturbed. For interactions between charged surfaces it is conceivable that the hydrophobic attraction due to the overlap of the depletion layers might very well dominate the resulting behaviour.

## 5. Ion-specific effects

In the preceding sections, ions were either treated as pointlike or as hard spheres. However, a large number of phenomena in colloid, polymer, and interface science that involve electrolytes show pronounced ion specificity, as categorized in the famous Hofmeister series [34–38].

Previous theoretical explanations invoked solvent structure effects [39–43], and surface-specific ion interactions [44, 45] or charge-regulation phenomena [46]. The presence of excess ionic polarizabilities was proposed to lead to corrections to the usual van der Waals interaction energy, which could be one of the factors determining ion-specific interactions [47–49].

How do we expect ion-specific effects to come into play on a microscopic level? At any charged surface, one has chemical groups which carry most of the surface charge, i.e., at which location the charge density is locally increased. The counterions (or any other oppositely charged molecule) will, due to Coulomb interactions, be on average quite close to these surface groups (in fact much closer than would be predicted according to Poisson–Boltzmann theory assuming a laterally homogeneous surface charge; compare section 3), and it seems natural to surmise that it is the interaction between oppositely charged chemical groups that will be most susceptible to chemical specificity. This is not to say that solvent effects (i.e. water structuring which of course differs for different ion types) is unimportant—on the contrary—but it does not make sense to separate solvent-induced effects from the bare interactions between oppositely charged groups. One experimental example where the specificity is exhibited very clearly is with AFM experiments for polyelectrolytes adsorbed on a variety of different substrates [28], where the plateau desorption force can be directly converted into the binding energy per unit length.

Fortunately, progress in the available quantum computational methodology allows us to calculate effective interactions between charged species in an essentially *ab initio* manner [50], including solvent effects [51]. As a prototype for the effects studied, we show in figure 4 *ab initio* results for the interaction between a sodium and a chlorine ion in vacuum. In figure 4(a) we show the resulting energy of interaction between the two ions as a function of their separation in units of $k_{\mathrm{B}}T$. The open diamonds are obtained using Hartree–Fock methods (HF), i.e. each electron sees a mean charge distribution due to the other electrons; otherwise the Schrödinger equation is explicitly solved for all 28 electrons involved (treating the nuclei as being fixed), using an expansion in TZV basis functions with added polarization and diffuse wavefunctions. The open stars denote results where electron correlations have been taken into account on the one-loop level (HF-MP2); the energy is slightly lower. One would expect most of the long-ranged attraction seen in figure 4(a) to be due to the Coulomb attraction between the separated charges on the two ions. To make that notion quantitative, we first have to find out how much charge is transferred between the two ions. In figure 4(b) we plot the ratio of the dipole moment of the whole charge distribution (including both ions in units of the elementary charge) and the ion–ion separation as a function of the separation. This ratio can be interpreted as the effective charge transferred between the two ions. It is seen that charge transfer is indeed almost perfect at large distances in which limit both ions are fully charged. For smaller distances, polarization effects lead to a decrease of the transferred charge. In figure 4(c) we show the same data as in figure 4(a) but with the Coulomb attraction $v(r) = -\ell_{\mathrm{B}}/r$ subtracted (note that the Bjerrum length in vacuum measures $\ell_{\mathrm{B}} = 55.73$ nm). Quite surprisingly, the resulting energy shows a pronounced attractive minimum of depth $\simeq -10\ k_{\mathrm{B}}T$ in a distance range $0.25\ \mathrm{nm} < D < 0.4\ \mathrm{nm}$. Both HF and MP2 calculations give roughly the same result; the difference between the two can be viewed as an estimate of the systematic error in the calculation due to the necessarily incomplete basis set. What is the reason for this quite strong attraction between the ions? Two contributions come to mind, namely the polarization attraction due to the charge-induced dipole interaction and the van der Waals interaction. Let us discuss both in some detail.

The static polarizability of the isolated ions can be calculated using the same *ab initio* methods by applying a small electric field and measuring the induced dipole moment (or by measuring the energy increase). We obtain $\alpha_{\mathrm{Cl}^-}/(4\pi\varepsilon_0) = 3.404\ \text{Å}^3$ within HF and

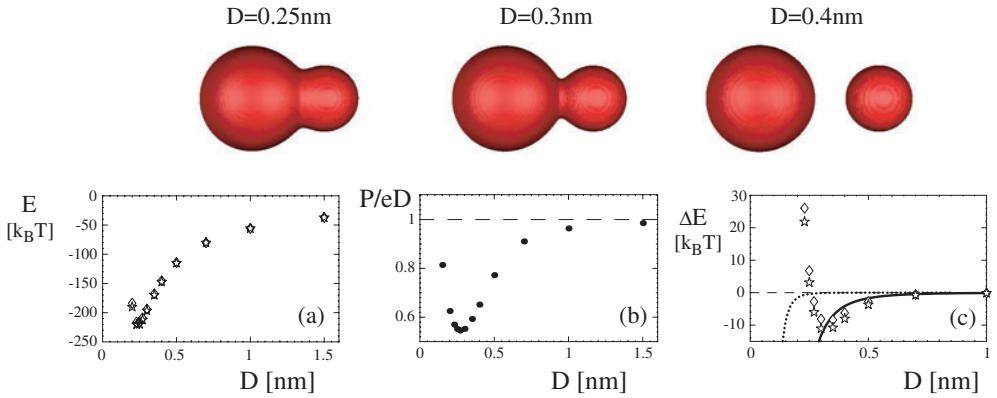


**Figure 4.** Top panel: surfaces of constant electron density (roughly corresponding to the density at the van der Waals surface) for three different values of the distance between a sodium (to the right) and a chlorine ion (to the left) in vacuum. (a) The interaction energy obtained using HF with a TZV basis set (open diamonds) and including electron correlations on the MP2 level (open stars). (b) Dipole moment divided by distance as a function of the ion distance, indicating that the two ions are fully charged for large separations. (c) The non-Coulombic interaction obtained by subtracting the Coulomb energy from the data in (a). Note that a deep minimum is present which can be explained by the charge-induced dipole interaction (solid curve) for large distances. The dispersion interaction (dotted curve) is irrelevant for all distances.

$\alpha_{Cl^-}/(4\pi\varepsilon_0) = 3.666$ Å$^3$ within HF-MP2 for the $Cl^-$ ion, and $\alpha_{Na^+}/(4\pi\varepsilon_0) = 0.132$ Å$^3$ within HF and $\alpha_{Na^+}/(4\pi\varepsilon_0) = 0.143$ Å$^3$ within HF-MP2 for the $Na^+$ ion. The charge-induced dipole interaction between the $Cl^-$ and $Na^+$ ions is, in units of $k_BT$ [52],

$$w_{ind}(r) = -\frac{\ell_B(\alpha_{Cl^-} + \alpha_{Na^+})}{8\pi\varepsilon_0 r^4} \tag{13}$$

and is plotted in figure 4(c) as a solid curve. It describes the ion–ion interaction quite well except for very small distances where the electron clouds overlap strongly. So it seems fair to say that the ionic interaction in vacuum is at large distances mostly dominated by polarization effects.

The dispersion interaction between two atoms has been calculated using quantum mechanical perturbation theory [53] and is given by (in units of $k_BT$)

$$w_{disp}(r) = -\frac{3\alpha_{Cl^-}\alpha_{Na^+} I_{Cl^-} I_{Na^+}}{2(4\pi\varepsilon_0)^2(I_{Cl^-} + I_{Na^+})r^6} \tag{14}$$

where the ionization energies of the two ions are measured in units of $k_BT$ also. For the ionization potentials we obtain, using the same level of HF-MP2, the results $I_{Cl^-} = 138.57\,k_BT$ and $I_{Na^+} = 1820.2\,k_BT$[1]. The resulting dispersion interaction is plotted in figure 4(c) as a dotted line. It is basically negligible for the whole relevant range of distances. This tells us that the attraction that appears in the quantum mechanical calculation is at large distances mostly due to polarization effects. It has to be considered as an important factor in the interaction

[1] It might be helpful to compare our *ab initio* calculations with experimental values. Note that for ions only few data are available in the literature. Our results for the polarizability and ionization potential of a neutral sodium atom, which are well tabulated, are $\alpha_{Na}/(4\pi\varepsilon_0) = 25.04$ Å$^3$ and $I_{Na} = 5.086$ eV, which have to be compared with the experimental values $\alpha_{Na}/(4\pi\varepsilon_0) = 23.6$ Å$^3$ and $I_{Na} = 5.139$ eV [52]. The agreement is sufficient for the present purpose. One notes the big differences between the data for ions and the corresponding neutral atoms. Approximating ionic properties by the neutral-atom data is therefore a bad idea. Other results for some neutral atoms and ions are given in table 1.

**Table 1.** *Ab initio* results for ionization energies $E_{\rm ion}$ and polarizabilities $\alpha$ for various atoms and ions in vacuum. The cavity radii $R_{\rm cav}$ are larger by a factor of 1.2 than the van der Waals radii. The effective ionic dielectric constant $\varepsilon$ and the excess polarizabilities $\alpha^{\infty}_{\rm exc}$ at large frequencies and at zero frequency $\alpha^{0}_{\rm exc}$ are calculated from the Clausius–Mossotti/Lorenz–Lorentz equation; see the text. The shift of the ionization energy in water, $\Delta E_{\rm ion}$, is calculated using a simple Born self-energy model. For conversion, note that 1 eV = 96.4516 kJ mol$^{-1}$ and 1 eV = 38.610 $k_{\rm B}T$. Numbers in parentheses are experimental values.

| | $E_{\rm ion}$ (eV) | $\frac{\alpha}{4\pi\varepsilon_0}$ (Å$^3$) | $R_{\rm cav}$ (Å) | $\varepsilon$ | $\frac{\alpha^{\infty}_{\rm exc}}{4\pi\varepsilon_0}$ (Å$^3$) | $\frac{\alpha^{0}_{\rm exc}}{4\pi\varepsilon_0}$ (Å$^3$) | $\Delta E_{\rm ion}$ (eV) |
|---|---|---|---|---|---|---|---|
| Li | 5.37 (5.39) | 24.9 (24.3) | | | | | |
| $Li^+$ | 75.0 | 0.022 | 0.72 | 1.186 | −0.040 | −0.18 | −29.7 |
| $Na^+$ | 47.1 | 0.14 | 1.14 | 1.32 | −0.11 | −0.72 | −18.8 |
| $K^+$ | 31.5 | 0.81 | 1.596 | 1.75 | 0.062 | −1.97 | −13.4 |
| $Fl^-$ | 3.54 | 1.01 | 1.632 | 1.90 | 0.195 | −2.10 | 4.37 |
| $Cl^-$ | 3.59 | 3.67 | 2.172 | 2.62 | 1.63 | −4.87 | 3.28 |
| Br | 13.6 (11.81) | 2.91 (3.05) | | | | | |
| $Br^-$ | 3.39 | 6.61 | 2.34 | 4.19 | 4.29 | −5.91 | 3.04 |
| $NO_3^-$ | 3.69 | 4.69 | 2.45 | 2.40 | 1.88 | −7.04 | 2.91 |
| $SCN^-$ | 2.42 | 7.48 | 2.62 | 3.14 | 4.08 | −8.45 | 2.72 |
| $H_2O$ | | 1.31 (1.45) | 1.93 | 1.669 (1.78) | | | |

between charged surfaces, since such additional interactions between ions and surfaces lead to charge regulation and thus to varying effective surface charges. Likewise, the interaction between ions in the bulk modifies the ionic activities and therefore gives an additional shift of the surface-group dissociation equilibrium. Clearly, this interaction is highly specific and different for different ion types, especially at small distances. A hand-waving explanation of why the very short-ranged properties of this interaction will be important is that oppositely charged ions are squeezed together such that the electron orbitals overlap to a degree where quantum mechanical effects come into play. This might be intuitively understood by looking at the electron density contours shown in the upper panel in figure 4. In all three pictures, the electron densities on the contour surfaces are the same and roughly correspond to the density on the van der Waals surfaces (the van der Waals radius for the $Cl^-$ ion is $R_{Cl^-} \simeq 0.181$ nm and for the $Na^+$ ion it is $R_{Na^+} \simeq 0.095$ nm). It is seen that for the range of distances where the attraction is strongest the electron distributions overlap. A similar short-ranged interaction between ions had been introduced in an ad hoc fashion in order to accurately fit activity coefficients of alkali halide solutions [54, 55], but we argue here that it is a general feature of oppositely charged groups; it is not restricted to simple ions but also applies to the interaction between macroscopic charged bodies. A similar interaction should also be present for the case of similarly charged ions, though here we would in general expect the effects to be small since the Coulomb repulsion in this case will make close contacts between ions unlikely in the general case. In previous theories which concentrated on water structure effects for electrolyte behaviour, the bare interionic potential has been typically regarded as rather structureless [42]. It might be interesting to reconsider such calculations by adding quantum mechanical potentials, such as we have calculated.

Conversely, it is important within our approach to critically check how the interaction we obtain will be modified in the presence of water. To do so we performed Hartree–Fock calculations using the so-called polarizable continuum model where the ions are embedded in spherical shells outside of which a dielectric medium with relative dielectric constant $\varepsilon = 78.39$ is assumed. The choice of the radii of these cavities is critical; we chose the cavity radii to be bigger than the van der Waals radii of the ions by a factor of 1.2. This means that the two dielectric cavities for the case of $Na^+$ and $Cl^-$ start touching at a distance

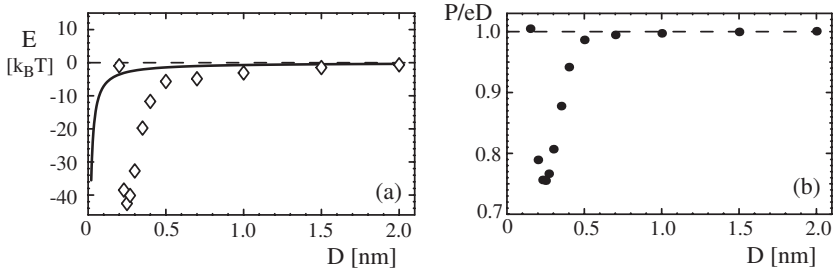


**Figure 5.** (a) The energy of interaction between a sodium and a chlorine ion obtained using Hartree–Fock methods and a polarizable continuum model with parameters representing liquid water. Open diamonds represent the full interaction energy in units of $k_B T$. The solid curve corresponds to the Coulomb interaction between two unit charges in a homogeneous material of relative dielectric constant $\varepsilon = 78.39$, which underestimates the true Coulomb attraction considerably. (b) Dipole moment divided by distance as a function of the ion distance, indicating that the two ions are fully charged already for intermediate separations.

of $D = 1.2(0.095\ \text{nm} + 0.181\ \text{nm}) = 0.331\ \text{nm}$. The Schrödinger equation is then solved taking into account the effects of polarization charges [51]. The open diamonds in figure 5(a) represent the full interaction obtained between the two ions. One notes that the long-ranged attractive tail has almost disappeared. The solid curve corresponds to the Coulomb interaction between two unit charges with a relative dielectric constant of $\varepsilon = 78.39$. This Coulomb potential is quite small, which is understandable since the Bjerrum length now takes the value $\ell_B \simeq 0.71$ nm. It is important to note that the true electrostatic interaction is quite involved because of the complicated geometry: for distances larger than $D = 0.331$ nm one has two separate spherical dielectric cavities which are immersed in a high-dielectric-constant background mimicking water. For smaller distances, the spherical cavities overlap. The Coulomb interaction between two charges inside the cavities shows a complicated crossover from a weak interaction at large distances, characterized by a Bjerrum length $\ell_B \simeq 0.71$ nm, to a strong interaction at distances smaller than the cavity overlap distance, where the Bjerrum length becomes closer to the vacuum value $\ell_B = 55.73$ nm. This is more or less what one sees in the data in figure 5(a). As a consequence, the short-ranged attraction is even stronger and now has a depth of 40 $k_B T$. It should be noted that this short-ranged attraction is mostly due to the modification of the Coulomb potential in the presence of dielectric boundaries (for similarly charged ions, the effective interaction will be predominantly repulsive).

What would we expect for the charge-induced dipole and the dispersion interaction in this case? To make progress we first need to evaluate the effective dielectric constant of the ion-containing cavity, which follows from the Clausius–Mossotti equation [56] (or the frequency dependent analogue, the Lorenz–Lorentz equation [57]) as

$$\varepsilon = \frac{2\alpha/(4\pi\varepsilon_0 R^3) + 1}{1 - \alpha/(4\pi\varepsilon_0 R^3)}. \tag{15}$$

For the chlorine ion with $R_{Cl^-} \simeq 0.2172$ nm and $\alpha_{Cl^-}/(4\pi\varepsilon_0) = 3.666\ \text{Å}^3$ one obtains $\varepsilon_{Cl^-} \simeq 2.62$, and for the sodium ion with $R_{Na^+} \simeq 0.114$ nm and $\alpha_{Na^+}/(4\pi\varepsilon_0) = 0.143\ \text{Å}^3$ one obtains $\varepsilon_{Na^+} \simeq 1.32$, where these numbers are equally valid in the static and dynamic cases. Other results for different atoms and ions are given in table 1. For the charge-induced dipole interaction what counts is the static excess polarizability of the ions in water, which again can be calculated from the inverted Clausius–Mossotti/Lorenz–Lorentz equation,

$$\alpha_{exc}/(4\pi\varepsilon_0) = R^3 \frac{\varepsilon_{ion} - \varepsilon_{water}}{\varepsilon_{ion} + 2\varepsilon_{water}}, \tag{16}$$

and is denoted by $\alpha^0_{\rm exc}$ and given in table 1. Since water has a much higher static dielectric constant than the ions, $\varepsilon^0_{\rm water} = 78.39$, it is clear that the excess static polarizability is negative and thus the charge-induced dipole contribution to the interaction energy is repulsive. It is therefore ruled out as a possible explanation for the observed attraction between the ions seen in the data in figure 5(a). For the dispersion interaction we have a static contribution, which is attractive but rather weak (since it is at most of the order of $3\,k_{\rm B}T$ at contact [52]) and a dynamic contribution. For the dynamic dispersion interaction what counts is the frequency dependent dielectric constant of the ions, given above, and of water, which follows from the refractive index $n \simeq 1.33$ as $\varepsilon^\infty_{\rm water} = n^2 \simeq 1.78$. According to the Lorenz–Lorentz equation (16), the excess polarizability is reduced, such that the dynamic dispersion interaction will be even smaller than the one in vacuum (which is shown in figure 4(c) as a dotted curve). To get explicit numbers for the dynamic excess polarizabilities of ions in water, we have calculated the high-frequency dielectric constant of water within our *ab initio* technique using the same method as for the ions. The result is $\varepsilon^\infty_{\rm water} = 1.669$ and thus smaller than the experimental value by 6% (see table 1). For consistency reasons, we have estimated the finite-frequency ion excess polarizabilities with the calculated value of the water dielectric constant. The results are given in table 1. The resulting excess polarizabilities are always smaller than the ones for in vacuum. We also estimate the ionization energies in the water environment using a simple Born self-energy argument. For the anion, the ionization energy is increased by the term

$$\Delta E_{\rm ion} = (\ell_{\rm B}^{\rm vac} - \ell_{\rm B}^{\rm water})/(2R_{\rm cav}) \tag{17}$$

which measures the electrostatic self-energy difference of a charged sphere in vacuum and in water. The vacuum Bjerrum length is given by $\ell_{\rm B}^{\rm vac} = 55.73$ nm and the Bjerrum length in water is $\ell_{\rm B}^{\rm water} = 0.71$ nm. For the cations, the ionization energy is reduced by the term

$$\Delta E_{\rm ion} = -(4-1)(\ell_{\rm B}^{\rm vac} - \ell_{\rm B}^{\rm water})/(2R_{\rm cav}) \tag{18}$$

which is the self-energy difference of a divalent and a monovalent charged sphere in vacuum and in water. The resulting numerical values are given in table 1. The effect of the ionization energy change on the dispersion interaction is roughly increasing the dispersion strength by a factor of two (this follows from the fact that the sum of ionization energies in the denominator of equation (14) is dominated by the larger cationic energy which therefore cancels the cationic energy in the numerator). The reduction of the polarizability in water however is larger than the increase of the ionization term, so in essence the dispersion interaction in water is even weaker than that in vacuum. Similarly to the situation in vacuum, therefore, the dispersion interaction is only a negligible contribution to the full interaction obtained within the *ab initio* calculation. As a main result, we find that, owing to the shape and size dependent crossover of the effective Coulomb interaction, the effective interaction between ions in a polarizable continuum medium is thus quite specific and depends sensitively on the shape and size of the ions.[2] It remains to be checked how these results will be modified if discrete water molecules are included in the calculation, but it seems likely that specific short-ranged interactions between oppositely charged chemical groups play an important role in the physics of strongly charged systems.

[2] A striking experimental example of counterion specificity is obtained for the cationic surfactant discussed in section 2. On exchanging the bromine ion in DDAB with a chlorine ion, the phase diagram changes dramatically and the phase coexistence disappears completely [9]. This is difficult to understand based on dispersion or polarization effects, since their combined contribution to the effective interionic potential in water is quite small. The reason for the big difference in the surfactant phase diagram is probably a steric coordination effect, allowing one of the ions to come into close contact with the cationic surfactant head region.

## 6. Summary and perspectives

Results from four different simulation techniques have been presented. The common motif among those calculations is the question about the properties of charged surfaces. On the smallest length scale, we showed results for the interaction between oppositely charged ions on the quantum chemical *ab initio* level. In vacuum, ions show some attractive interaction which can be understood by invoking charge-induced dipole effects. In a dielectric medium, on the other hand, the interaction is dominated by the dielectric effect, which is highly ion specific because of the strong influence of the ionic geometry. These effects will influence the dissociation equilibrium of surface groups. Dispersion interactions between ions are found to be rather small. Note that the *ab initio* calculations are done at zero temperature. Within all-atom molecular dynamics simulations, finite temperature and hydration effects can be accurately studied. We demonstrated this for the water density profile at a single hydrophobic surface which shows pronounced depletion in agreement with recent experiments. Note that the quality of MD simulations of course depends on the quality of the force fields implemented, and it is here where *ab initio* calculations can be used to make the assumptions inherent in MD simulations more realistic. In MD simulations, the true Newtonian dynamics is simulated, which means that a lot of computer time is used in taking into account the small-scale dynamics of water. This is important for certain applications, but limits the maximal size and maximal time span of the simulation. In order to get hydrodynamic and large-scale properties right, one has to resort to coarse grained simulation techniques, where water is replaced by some continuum medium (note that in principle the water structure at surfaces could be put in by choosing non-local dielectric functions at the surface). We showed results for the counterion distribution at structured surfaces using stochastic Brownian dynamics simulations (which also give dynamical properties such as ionic mobilities) and for smooth, idealized surfaces using Monte Carlo techniques which allow us to quantitatively compute the deviations from mean-field (Poisson–Boltzmann) predictions.

As we tried to bring out in this short review, a full understanding of charged surfaces requires the combination of different simulation techniques. We have only started to bridge the gap between the quantum mechanical world at small distances and the mesoscopic world of primitive models (where ions are replaced by hard spheres, and the solvent by a dielectric constant plus possibly effective interactions between the ions). What needs to be fully elucidated is the coupling between water structure close to ions and at charged surfaces and the effective interaction between such charged groups, which probably involves effective many-body interactions. Experimentally evidenced ion-specific effects will turn out to be a stringent test for such theories.

## Acknowledgments

It is a pleasure to thank my collaborators Y W Kim, S Mamatqulov, A Moreira, A Naji and H Orland with whom I have been working on charged surfaces. I also thank M Dubois, W Kunz, T Zemb for discussions and for sending data and pictures. This work was financially supported by Deutsche Forschungsgemeinschaft (DFG) via the grants SFB 486, SFB 563, German–French Network, and by the Fonds der Chemischen Industrie.

## References

[1] Holm C, Kekicheff P and Podgornik R (ed) 2001 *Electrostatic Effects in Soft Matter and Biophysics* (Dordrecht: Kluwer)
[2] Levin Y 2002 *Rep. Prog. Phys.* **65** 1577
[3] Grosberg A Y, Nguyen T T and Shklovskii B I 2002 *Rev. Mod. Phys.* **74** 329
[4] Hansen J P and Löwen H 2000 *Annu. Rev. Phys. Chem.* **51** 209

[5] Belloni L 2000 *J. Phys.: Condens. Matter* **12** R549
[6] Guldbrand L, Jönson B, Wennerström H and Linse P 1984 *J. Chem. Phys.* **80** 2221
[7] Dubois M and Zemb T 1991 *Langmuir* **7** 1352
[8] Zemb T, Gazeau D, Dubois M and Gulik-Krzywicki T 1993 *Europhys. Lett.* **21** 759
[9] Dubois M, Zemb T, Fuller N, Rand R P and Parsegian V A 1998 *J. Chem. Phys.* **108** 7855
[10] Khan A, Jönsson B and Wennerström H 1985 *J. Phys. Chem.* **89** 5180
[11] Wennerström H, Khan A and Lindman B 1991 *Adv. Colloid Interface Sci.* **34** 433
[12] Moreira A G and Netz R R 2001 *Phys. Rev. Lett.* **87** 078301
[13] Netz R R 2001 *Eur. Phys. J.* E **5** 557
[14] Moreira A G and Netz R R 2002 *Eur. Phys. J.* E **8** 33
[15] Moreira A G and Netz R R 2000 *Europhys. Lett.* **52** 705
[16] Moreira A G and Netz R R 2002 *Europhys. Lett.* **57** 911
[17] Rouzina I and Bloomfield V A 1996 *J. Phys. Chem.* **100** 9977
[18] Shklovskii B I 1999 *Phys. Rev.* E **60** 5802
[19] Gouy G 1910 *J. Physique* **IX** 457
[20] Chapman D L 1913 *Phil. Mag.* **25** 475
[21] Andelman D 1995 *Handbook of Biological Physics* ed R Lipowsky and E Sackmann (Amsterdam: Elsevier)
[22] Netz R R 2003 *Phys. Rev. Lett.* **91** 138101
[23] Stillinger F H 1973 *J. Solut. Chem.* **2** 141
[24] Lee C Y, McCammon J A and Rossky P J 1984 *J. Chem. Phys.* **80** 4448
[25] Harder P, Grunze M, Dahint R, Whitesides G M and Laibinis P E 1998 *J. Phys. Chem.* B **102** 426
[26] Chan Y-H M, Schweiss R, Werner C and Grunze M 2003 *Langmuir* **19** 7380
[27] Kreuzer H J, Wang R L C and Grunze M 2003 *J. Am. Chem. Soc.* **125** 8384
[28] Friedsam C, Del Campo Becares A, Jonas U, Seitz M and Gaub H E 2004 *New J. Phys.* **6** 9
[29] Steitz R, Gutberlet T, Hauss T, Klösgen B, Krastev R, Schemmel S, Simonson A C and Findenegg G H 2003 *Langmuir* **19** 2409
[30] Schwendel D, Hayashi T, Dahint R, Pertsin A J, Grunze M, Steitz R and Schreiber F 2003 *Langmuir* **19** 2284
[31] Jensen T R, Ostergaard Jensen M, Reitzel N, Balashev K, Peters G H, Kjaer K and Bjornholm T 2003 *Phys. Rev. Lett.* **90** 086101
[32] Granick S 2004 at press
[33] Mamatkulov S I, Khabibullaev P K and Netz R R 2004 *Langmuir* at press
[34] Hofmeister F 1888 *Naunin-Schmiedebergs Archiv für Experimentelle Pathologie und Pharmakologie (Leipzig)* **24** 247
[35] Conway B E 1995 *Electrochim. Acta* **40** 1501
[36] Cacace M G, Landau E M and Ramsden J J 1997 *Q. Rev. Biophys.* **3** 241
[37] Ruckenstein E and Manciu M 2003 *Adv. Colloids Interf. Sci.* **105** 177
[38] Maheshwari R, Sreeram K J and Dhathathreyan A 2003 *Chem. Phys. Lett.* **375** 157
[39] Marcelja S, Mitchell D J, Ninham B W and Sculley M J 1977 *J. Chem. Soc. Faraday Trans.* II **73** 630
[40] Podgornik R, Cevc G and Zeks B 1987 *J. Chem. Phys.* **87** 5957
[41] Kusalik P G and Patey G N 1990 *J. Chem. Phys.* **92** 1345
[42] Lyubartsev A P and Laaksonen A 1997 *Phys. Rev.* E **55** 5689
[43] Jungwirth P and Tobias D 2001 *J. Phys. Chem.* B **105** 10468
[44] Stern O 1924 *Z. Elektrochem.* **30** 508
[45] Podgornik R 1989 *J. Chem. Phys.* **91** 5840
[46] Spalla O and Belloni L 1995 *Phys. Rev. Lett.* **74** 2515
Belloni L and Spalla O 1996 *Ber. Bunsenges. Phys. Chem.* **100** 905
[47] Boström M, Williams D R M and Ninham B W 2001 *Phys. Rev. Lett.* **87** 168103
[48] Netz R R 2000 *Eur. Phys. J.* E **3** 131
Netz R R 2001 *Eur. Phys. J.* E **5** 189
[49] Kunz W, Belloni L, Bernard O and Ninham B W 2004 *J. Phys. Chem.* B **108** 2398
[50] Schmidt M W, Baldrige K K, Boatz J A, Elbert S T, Gordon M S, Jensen J J, Koseki S, Matsunaga N, Nguyen K A, Su S, Windus T L, Dupuis M and Montgomery J A 1993 *J. Comput. Chem.* **14** 1347
[51] Tomasi J and Persico M 1994 *Chem. Rev.* **94** 2027
[52] Israelachvili J 1991 *Intermolecular and Surface Forces* (London: Academic)
[53] London F 1937 *Trans. Faraday Soc.* **33** 8
[54] Rasaiah J C 1970 *J. Chem. Phys.* **52** 704
[55] Ursenbach C P, Wei D and Patey G N 1991 *J. Chem. Phys.* **94** 6782
[56] Mossotti P F 1847 *Bibl. Univ. Modena* **6** 193
[57] Böttcher C J F 1973 *Theory of Electric Polarization* (Amsterdam: Elsevier)